Analytic description of photoeffect from atomic ions

David J. Botto, James McEnnan,* and R. H. Pratt
Department of Physics, University of Pittsburgh, Pittsburgh, Pennsylvania 15260
(Received 20 April 1978)

Analytic expressions previously derived for neutral atoms permit the accurate prediction of inner-shell nonrelativistic dipole photoeffect cross sections for positively charged atomic ions. The simple dependence of these cross sections on nuclear charge Z and ionic charge Z_i results from scaling properties of self-consistent central potentials in the interior of the atom. Comparisons are made with numerical calculations of the same cross sections.

I. INTRODUCTION

We wish to present a simple systematic analytic description of photoeffect from atomic ions based on the behavior of the self-consistent potential in the interior of the atom. We employ results of a previous calculation of screened photoeffect cross sections from neutral atoms,[1] derived using an analytic perturbation theory which we have developed for the description of inner bound and continuum wave functions.[2,3] We find that for K- and L-shell photoeffect cross sections from ions our analytic expressions agree with single-electron numerical calculations for essentially all energies except for a small region near threshold (tens of eV for the K shell and a keV for the L shell for neutral and lightly ionized atoms, and substantially better as the degree of ionization increases). Further, this analytic approach provides an explanation for the dependence of these cross sections on nuclear charge Z and ionic charge Z_i.

Knowledge of photoeffect cross sections from atomic ions is of interest in high-temperature plasma studies, solar physics, and astrophysics. Because of the practical difficulties in producing significant quantities of multicharged positive ions in the laboratory only a few direct measurements of the photoeffect cross sections for these cases are available.[4,5] Recently several sample numerical calculations of ionic photoeffect cross sections have been reported.[6-13] However such calculations, even of large scale, do not necessarily emphasize or explain simple regularities which are present in these cross sections. It is therefore desirable to consider analytic approximations from which general systematic trends can be extracted, such as the dependence on nuclear charge, degree of ionization, photon energy, etc. One analytic approach, neglecting energy dependence, has been reported,[14] and we shall discuss its validity. While previous discussions have concentrated primarily on outer shells at energies not too far above threshold, we are here concerned with inner shells over a larger range of energies. We reproduce and explain some of the general conclusions obtained from numerical studies.

The basic theory which we employ, as well as the needed explicit expressions for K- and L-shell photoeffect cross sections, is given in Refs. 1-3. Briefly, our approach is based upon the expansion of the potential in the interior of the atom as a series of the form

$$V(r)=(-a/r)[1+V_1(\lambda r)+V_2(\lambda r)^2+V_3(\lambda r)^3+\cdots], \tag{1}$$

where $a=\alpha Z$ (α is the fine structure constant and Z the nuclear charge), here λ is a small Z-dependent parameter characterizing the screening, and the potential expansion coefficients V_k, which will depend both on Z and the ionic Z_i, are of order unity. We choose units such that $\hbar=c=m_e=1$.

Given this expansion of the potential, valid at distances which contribute to the inner-shell photoeffect matrix elements, analytic forms for wave functions and normalizations may be obtained as series in λ. In the nonrelativistic dipole approximation the total photoeffect cross section for ejection of electrons of momentum k from the subshell specified by quantum numbers n and l is given by

$$\sigma_{nl}=(2\pi)^2\alpha\omega\tfrac{2}{3}(4\pi)^2[(l+1)|\langle k,l+1|r|n,l\rangle|^2 + l|\langle k,l-1|r|n,l\rangle|^2],$$

where within this analytic perturbation theory

$$|\langle k,l'|r|n,l\rangle|^2=(N_{nl}/N_{nl}^c)^2|\langle k_c,l'|r|n,l\rangle| \times[1-\lambda^2V_2\chi_{nl}^2(\nu) -\lambda^3V_3\chi_{nl}^3(\nu)-\cdots], \tag{2}$$

and $\langle k_c,l'|r|n,l\rangle$ is the corresponding point Coulomb matrix element evaluated at the same photon energy ω for ejection of an electron of momentum k_c. $(N_{nl}/N_{nl}^c)^2$, the bound-state normalization screening corrections, is the square of the ratio of screened to point Coulomb bound-state normalization. The χ_{nl}^k, given analytically in Ref. 1, are

screening corrections resulting from modification of continuum normalizations and continuum and bound-state wave-function shapes; they are simple elementary functions of ω/T_c, $\nu \equiv n/(\omega/|T_c| - 1)^{1/2}$ where the Coulomb bound-state energy $T_c = -a^2/2n^2$.

In Figs. 1 and 2 we display χ^2_{nl} and χ^3_{nl} as a function of $\omega/|T_c|$ for the K and L shells. At high photon energies the χ^k_{nl} vanish, so the only effect of screening in this limit is due to the change in the bound-state normalizations. This is precisely the conclusion obtained from the normalization screening theory of photoeffect.[15] For lower photon energies the corrections become quite large. Although the χ^k_{nl} diverge as $\omega/|T_c| \to 0$, for any physical process $\omega \geq |T_s| > 0$, with T_s the screened binding energy, and the corrections are still finite at threshold. Care must be used to insure the proper analytic continuation of $|\langle k_c l'|r|n, l\rangle|^2$ is employed below the point Coulomb threshold.[16]

The screened bound-state normalizations N_{nl} are given by

$$\begin{aligned} N_{10} &= N^c_{10}[1 - \tfrac{3}{2}V_2(\lambda/a)^2 - \tfrac{11}{2}V_3(\lambda/a)^3], \\ N_{20} &= N^c_{20}[1 - 24V_2(\lambda/a)^2 - 328V_3(\lambda/a)^3], \\ N_{21} &= N^c_{21}[1 - 30V_2(\lambda/a)^2 - 320V_3(\lambda/a)^3], \end{aligned} \tag{3}$$

where

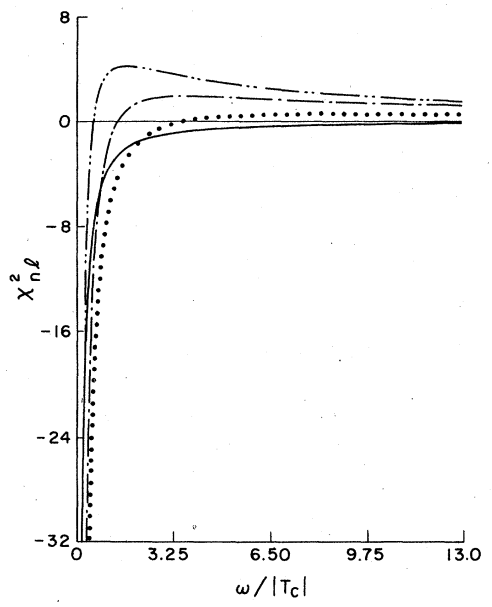

FIG. 1. Second-order screening corrections χ^2_{nl} resulting from modifications of continuum normalizations, and continuum and bound wave-function shapes, as a function of the ratio of photon energy to point Coulomb binding energy. The solid line is the K-shell correction, the dotted line is the L_I correction and the dashed lines (-·-·-, -·-·-·-) are the $L_{II}+L_{III}$ ($l \to l+1$, $l \to l-1$) corrections, respectively.

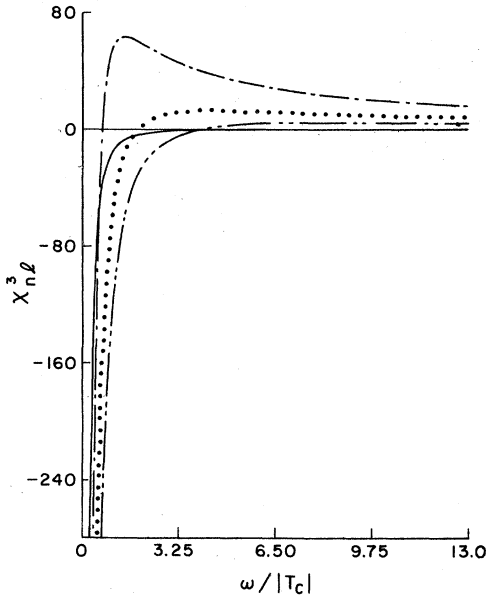

FIG. 2. Third-order screening corrections χ^3_{nl}. Otherwise the same as Fig. 1.

$$N^c_{nl} = \left(\frac{2a}{n}\right)^{l+3/2} \frac{1}{(2l+1)!}\left(\frac{(n+l)!}{2n(n-l-1)!}\right)^{1/2} \tag{4}$$

is the point Coulomb normalization. Further, the cross section (2) is subject to energy conservation,

$$\begin{aligned} E_f &= \omega + T_s \\ &= \omega - a^2/2n^2 - V_1\lambda a + \tfrac{1}{2}V_2\lambda^2[-3n^2 + l(l+1)] \\ &\quad - (n^2V_3\lambda^3/2a)[5n^2 + 1 - 3l(l+1)] + \cdots, \end{aligned} \tag{5}$$

where E_f is the kinetic energy of the photoelectron and T_s is the bound-state energy.

From Eqs. 2–5 we see that, assuming acceptable convergence of the various series, a complete analytic description of screened photoeffect cross sections is available once the potential expansion coefficients V_k and the screening parameter λ are specified. In the Sec. II we will discuss the behavior and determination of these quantities. In Sec. III we examine the resulting predictions for ionic photoeffect cross sections.

II. CHARACTERIZATION OF IONIC AND NEUTRAL POTENTIALS

Our work utilizes the self-consistent neutral-atom potentials tabulated by Herman and Skillman[17]; we generated the needed ionic potentials with the Herman-Skillman code. Since only the product $\lambda^k V_k$ occurs in our expansion of the potential (1) we must specify λ before we can give the V_k which characterize the potential. We have observed that for suitably chosen $\lambda(Z)$ the V_k which describe the

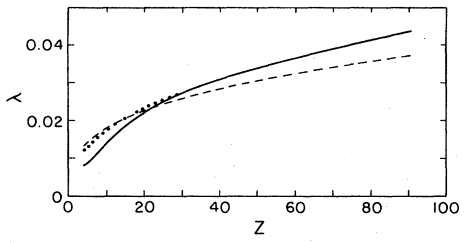

FIG. 3. Screening parameter λ as a function of the nuclear charge Z (solid line). For comparison we give the Thomas-Fermi (dashed line) choice for λ as well as the curve $\lambda = 0.9\alpha Z^{0.42}$ (dotted line).

neutral-atom potentials are largely independent of Z. This implies that for such $\lambda(Z)$, $V(Z,r)/V^c(Z,r) = f(\lambda r)$, where $V^c(Z,r) = -a/r$ is the point Coulomb potential—thus depending on Z and on r only as one universal function of the combination λr. This is true by definition for the Yukawa potential $V^Y/V^c = e^{-\lambda r}$. It is also true for the Thomas-Fermi potential with $\lambda = 1.13\alpha Z^{1/3}$. What we observe is that the Herman-Skillman (HS) potentials exhibit a similar scaling in the interior of the atom, but rather than $\lambda \sim Z^{1/3}$ as in the Thomas-Fermi (TF) model, we find that for high Z, $\lambda \sim Z^{0.42}$. We show in Fig. 3 the choice for $\lambda(Z)$ we have used in this paper, in which, for simplicity, since only the product $\lambda^k V_k$ is defined, we required $V_2 \equiv$ constant (0.75) for neutral atoms. The difference in slope (but not

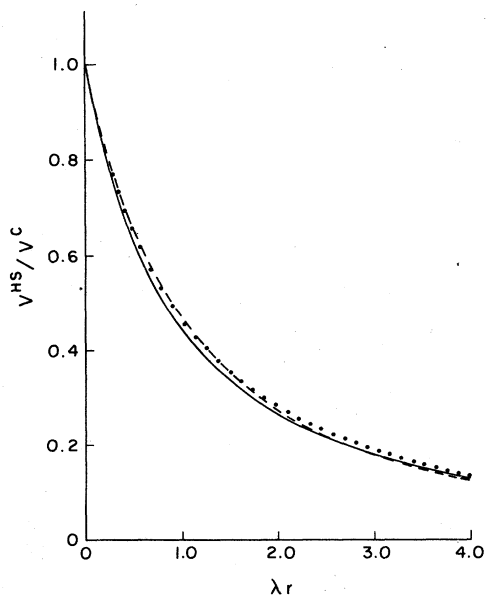

FIG. 4. Ratio of screened (HS) to point Coulomb potentials as a function of λr. The solid line is for neutral argon, the dotted line is for neutral tin and the dashed line for neutral gold.

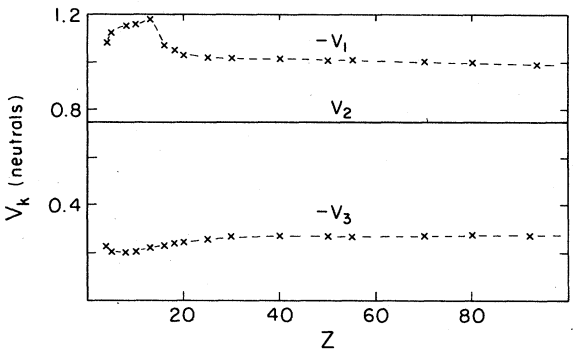

FIG. 5. First three potential expansion coefficients: $-V_1$ (solid line), V_2 (dotted line), and $-V_3$ (dashed line) for the neutral atoms. Z is the nuclear charge.

over-all constant) from Thomas-Fermi is significant. In Fig. 4 we demonstrate the extent of scaling of V^{HS}/V^c with this choice of λ, and we see that within the interior of the atom the ratio is fairly well represented by a universal curve.

The resulting neutral V_k are shown in Fig. 5. They are quite constant as asserted, although with some variation for low Z. [$V_2 \equiv 0.75$ was imposed to determine λ, while alternatively we could have chosen $\lambda(Z)$ to maximize the scaling of V/V^c in the interior of the atom. By requiring $V_2 \equiv 0.75$, the scaling in the interior region is better for high Z elements than for low Z elements.] Given λ, the V_k were determined by a direct least squares fit to $(V - V^c)/V^c$ over the range $0 < r < \lambda^{-1}$, keeping only as many terms (three) as correspond to the order-of-perturbation theory which we will retain in our subsequent analytic calculation. This method differs from that described in Ref. 2: the particular analytic form used there is not flexible enough to accurately fit the variations in sequences of ionic self-consistent potentials. With the present procedure, values of the V_k may change somewhat if higher orders in λ or a different radial range is considered,[18] but the resulting wave functions are a good approximation for any given order in λ and range. Furthermore, these fits accurately reflect the changes in the potential shape as the degree of ionization varies. Since in fact $\lambda(Z)$ was determined from V_2, an iterative procedure was used to determine λ and the neutral V_k.

For ionic potentials of nuclear charge Z and degree of ionization Z_i, we have used $\lambda(Z)$ as determined for the neutral potentials and then determined the ionic $V_k(Z, Z_i)$. We have noticed that the ionic $V_k(Z, Z_i)$ appear to depend only on the ratio Z_i/Z. These results are displayed in Fig. 6, where a sense of the spread in the V_k for fixed Z_i/Z is given by the error bars; this scaling breaks down for low Z. This implies that $rV(r)/a$ is a

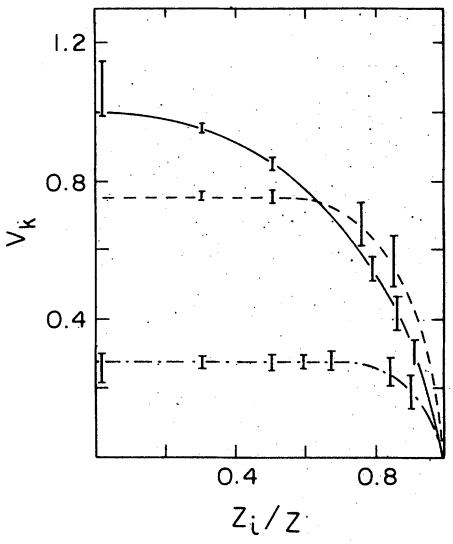

FIG. 6. Ionic potential expansion coefficients: $-V_1$ (solid line), V_2 (dotted line), and $-V_3$ (dashed line) as a function of the ratio Z_i/Z (of the degree of ionization to nuclear charge).

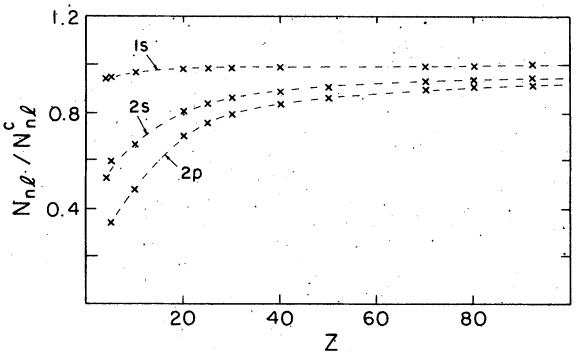

FIG. 7. Ratio of screened to point Coulomb bound-state normalizations for neutral atoms. The solid line is the K shell, the dotted line is the L_I subshell and the dashed line is the $2p$ subshell normalization ratio. Z is the nuclear charge.

function only of λr and of Z_i/Z.[19]

There are features of Fig. 6 which merit comment. First, for totally ionized atoms ($Z_i = Z$) the V_k vanish: the potential reduces to the corresponding point Coulomb potential in this limit. For low degrees of ionization (small Z_i/Z) V_2 and V_3 are relatively constant; as Z_i/Z increases V_2 and $-V_3$ decrease and finally for $Z_i = Z$ vanish. On the other hand, $-V_1$ decreases slowly for low degrees of ionization and more rapidly for higher degrees of ionization. In our expansion (1) the term containing V_1 is the shift in the potential at the origin due to the exterior charge distribution. Each atomic electron contributes to this as e^2/R, where R characterizes its orbit. The changes in V_1 when inner electrons are removed are larger than when outer electrons are removed, but even outer electrons contribute to V_1, as Fig. 6 shows. V_2 and V_3 characterize the shape of the potential in the interior of the atom and hence are mainly determined by the inner electron-charge distribution. For low degrees of ionization, only removing exterior electrons, the shape of the potential in the interior region of the ion will be essentially the same as that of the neutral atom. Thus V_2 and $-V_3$ will decrease only when inner electrons are removed, i.e., for highly ionized atoms, ionized into the L shell for light and intermediate Z, into the M shell for high Z.

To discuss the photoeffect matrix elements, we need not only the V_k but also the bound-state normalizations obtained from them via Eq. (3). The large coefficients (and relatively poor convergence) of these series for the L shell warrants some separate discussion, based on our knowledge of the V_k. It is apparent from Eq. (3) that these normalizations do not scale in Z_i/Z, as the V_k coefficients are multiplied by factors in λ/a. However, for large Z_i/Z the V_k are small and Eq. (3) is acceptable—these highly ionized cases do not deviate too greatly from point Coulomb values. For small Z_i/Z, V_2 and V_3 are relatively constant and so also the normalizations, which are equal to the neutral atom values, which we give in Fig. 7. If we use Eq. (3) for $Z_i/Z \geq 0.6$ and the neutral atom values of Fig. 7 for $Z_i/Z < 0.6$ we do not make errors in the normalization of more than 2%.

III. PREDICTIONS FOR PHOTOEFFECT

Once the V_k and the normalizations are tabulated, photoeffect cross sections can be obtained. And further, from general features of the V_k, general features of the cross sections can be understood. From the energy conservation relation Eq. (5) we see that the major screening correction to the threshold energy position is due to the V_1 term. For a given Z, $|V_1|$ (measuring the change in potential at the origin due to the presence of atomic electrons) decreases monotonically and at an increasing rate as the degree of ionization increases, so that as the degree of ionization increases the threshold energy for photoeffect increases monotonically and at an increasing rate, until the point Coulomb threshold energy is reached. We further have seen that for given Z, initially V_2 and V_3 (which characterize screening corrections to the potential shape in the interior of the atom) remain virtually constant as Z_i increases from $Z_i = 0$.

Since screening corrections through third order in λ are determined completely by V_2 and V_3 [see Eq. (2)], except for a shift in the threshold energy, the removal of outer-shell electrons does not appreciably affect inner-shell photoeffect cross sections. As the degree of ionization continues to increase the $|V_k|$ drop toward zero, the normalizations tend toward the point Coulomb values [Eq. (3)], and the screening corrections tend toward zero [Eq. (2)], so the cross sections go to their respective point Coulomb values. We may also note that at photon energies well above threshold (several times the binding energy of the subshell from which the photoelectron is ejected) the product $\lambda^k\chi^k_{nl}$ of Eq. (2) vanish, and the screening corrections to the cross sections are entirely due to the changes in the bound-state normalizations.[15] In this limit the ratio of cross sections is

$$\frac{\sigma_{nl}(Z,Z_i)}{\sigma_{nl}(Z',Z_i')}=\left(\frac{N_{nl}(Z,Z_i)}{N^c_{nl}(Z)}\,\frac{N^c_{nl}(Z')}{N_{nl}(Z',Z_i')}\right)^2\frac{\sigma^c_{nl}(Z,\omega)}{\sigma^c_{nl}(Z',\omega)}. \tag{6}$$

At appreciably higher-photon energies this ratio becomes independent of energy, because in the high-energy-limit Coulomb cross sections for photoeffect from a given shell have the same energy dependence, independent of nuclear charge.[20] If we fix Z ($Z'=Z$), the result reduces to

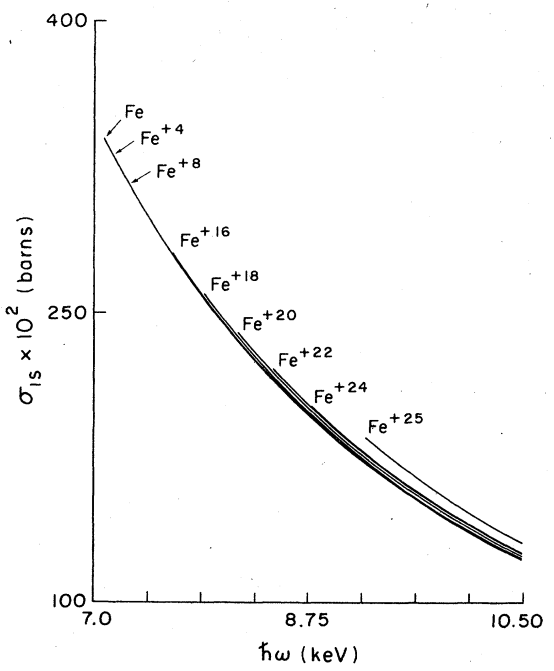

FIG. 8. K-shell photoeffect cross sections for various ions of iron. The cross section is in barns. The photon energy ω is in keV.

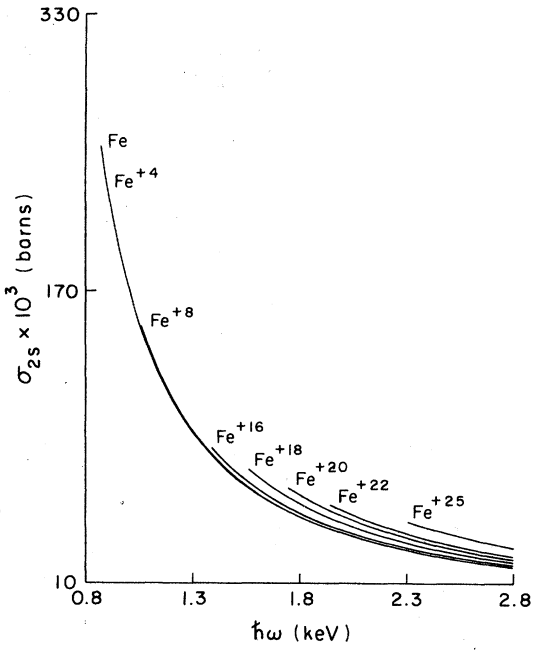

FIG. 9. The $L_{\rm I}$ photoeffect cross sections for various ions of iron. Otherwise the same as Fig. 8.

$$\frac{\sigma_{nl}(Z,Z_i)}{\sigma_{nl}(Z,Z_i')}=\left(\frac{N_{nl}(Z,Z_i)}{N_{nl}(Z,Z_i')}\right)^2, \tag{7}$$

so that in the high-energy limit the ratio of cross sections in an isonuclear sequence is completely determined by the square of the ratio of bound-state normalizations. For low degrees of ionization, where the normalizations are essentially the neutral values (V_2 and V_3 constant), the cross sections remains identical.

Figs. 8 and 9 show the photoeffect cross sections as predicted by our analytic approach for the iron isonuclear sequence. Figure 8 displays the K-shell cross sections while Fig. 9 displays the $L_{\rm I}$ subshell cross sections. We see for the K-shell cross section that aside from the shift in the threshold energy the cross sections are virtually identical—the cross section for Fe^{+24} differs only by a few percent from the neutral cross section. For the L_I cross section the cross sections are virtually identical for $Z_i<16$. As Z_i increases beyond 16 (corresponding to the removal of electrons whose principal quantum number is equal to 2), the cross sections increase. Thus, as had been asserted by Manson and others,[6-14] removal of outer-shell electrons, whose principal quantum number is greater than that characterizing the shell from which the photoelectron is ejected, does not have any significant effect on inner-shell photoeffect cross sections beyond causing a shift of the thres-

TABLE I. Comparison of our analytic results for the K, L_{I}, and $L_{\mathrm{II}}+L_{\mathrm{III}}$ shells σ_{an}, with numerical values for the nonrelativistic dipole cross section σ_{num}, with the values of the normalization screening theory σ_{NS} and with the point Coulomb values σ_C. T_C is the point Coulomb binding energy, T_B is the Herman-Skillman ground-state binding energy, and ω is the photon energy. All energies are in keV. All cross sections are in barns.

Z	Z_i	State	ω	σ_{num}	σ_{an}	σ_{NS}	σ_C
23	5	$1s$	5.497	4.467(4)	4.388(4)	4.682(4)	4.844(4)
		$T_C=$ 7.19	8.0	1.659(4)	1.661(4)	1.735(4)	1.795(4)
		$T_B=$ 5.487	30.0	3.947(2)	3.935(2)	3.974(2)	4.112(2)
		$2s$	1.5	4.792(4)	4.932(4)	5.545(4)	8.063(4)
		$T_C=$ 1.80	2.0	2.758(4)	2.735(4)	3.077(4)	4.475(4)
		$T_B=$ 0.7049	10.0	6.564(2)	6.538(2)	6.647(2)	9.665(2)
53	35	$1s$	34.0	5.905(3)	5.877(3)	6.015(3)	6.119(3)
		$T_C=$38.2	37.0	4.697(3)	4.708(3)	4.809(3)	4.892(3)
		$T_B=$33.75	50.0	2.120(3)	2.102(3)	2.134(3)	2.171(3)
		$2p$	6.44	6.749(4)	6.596(4)	7.232(4)	9.430(4)
		$T_C=$ 9.55	10.0	1.838(4)	1.814(4)	1.930(4)	2.516(4)
		$T_B=$ 6.43	20.0	2.063(3)	2.070(3)	2.115(3)	2.757(3)

hold energy.

We have made extensive comparisons of our analytic results with single-electron nonrelativistic dipole numerical results. Because the differences are small we cannot accurately display the comparison in Figs. 8 and 9 and we present a sample of this data in Table I. We also give the cross sections from the normalization screening theory and the point Coulomb cross sections. Our results for the K-shell cross sections agree to within 2% at photon energies of 10 eV above threshold. As the energy increases our results improve. For low Z and Z_i the corrections due to wave-function shapes and continuum normalizations are still of the order of 1% even at five times the binding energy. As Z and/or Z_i increases these effects decrease. For higher shells our results are not as good near threshold for low Z and Z_i. But as the energy increases they improve. As the energy, nuclear charge Z, and degree of ionization increase deviations from point Coulomb results, other than bound-state normalization efforts, diminish.

In Table II we show a comparison of our analytic results with a simpler prescription due to Huebner, Argo, and Ohlsen,[14] who have proposed an energy independent Z_{eff}^4 scaling of the ionic photoelectron cross section based upon Kramer's formula. We show the ratio of ionic to neutral cross sections for three ions of iron at two energies each. We display results from our analytic approach, numerical calculations and the approach of Huebner *et al.* Following earlier authors they proposed an effective Z which would vary from the neutral Z—effective only if electrons from the same shell were removed. We see that in the cases considered, Huebner *et al.* have no shift for the K-shell cross section, whereas for $Z_i=21$ the cross section for the ion is 2% higher than that for the neutral. For the L-shell cross sections as outer electrons are removed ($Z_i \geq 16$) the ionic cross section

TABLE II. Comparison of the ratio of photoeffect cross sections from ion to photoeffect from neutrals for three ions of iron (Z_i is the degree of ionization). num denotes the numerical single-particle nonrelativistic dipole result, an denotes our analytic theory, and H denotes the result of Huebner *et al.* All energies are in keV.

Z_i	Shell	ω	$(\sigma^i/\sigma^n)_{\mathrm{num}}$	$(\sigma^i/\sigma^n)_{\mathrm{an}}$	$(\sigma^i/\sigma^n)_H$
4	$1s$	8.3	1.00	1.00	1.00
16			1.01	1.00	1.00
21			1.02	1.02	1.00
4		10.3	1.00	1.00	1.00
16			1.00	1.00	1.00
21			1.02	1.02	1.00
4	$2s$	1.85	1.00	1.00	1.00
16			1.05	1.05	1.00
21			1.30	1.31	1.36
4		3.0	1.00	1.00	1.00
16			1.04	1.04	1.00
21			1.25	1.26	1.36
4	$2p$	1.8	1.00	1.00	1.00
16			1.05	1.05	1.00
21			1.38	1.39	1.36
4		5.0	1.00	1.0	1.00
16			1.04	1.05	1.00
21			1.30	1.30	1.36

has increased by about 5% over the neutral value. For a given Z_i as the photon energy increases the ratio of cross sections shows a few percent drop. This energy dependence is not found in the work of Huebner *et al.* For energies not too far above threshold the work of Huebner *et al.* agrees to within 8% of the numerical values, deviating with increasing energy. Our results, on the other hand, agree to within 2% and improve as the energy continues to increase.

This points out that the present theory has predictive powers for the ratio of cross sections near threshold even though it does not give an accurate numerical value for the cross sections in that case. The reason for this is, as noted earlier, for low degrees of ionization the coefficients V_2 and V_3 are independent of the degree of ionization.

In summary, we have shown that the analytic perturbation theory for screened Coulomb potentials may be used to accurately predict inner-shell nonrelativistic dipole photoeffect cross sections for positively charged atomic ions. This illustrates the general usefulness of this theory in describing inner-shell processes whose matrix elements are dominated by the region near the origin. Other such processes include nuclear radiative electron capture, ionization in nuclear capture, bremsstrahlung, etc. We have also recently applied the analytic theory to the study of bound-bound transition matrix elements.[21]

ACKNOWLEDGMENTS

We would like to thank Dr. S. T. Manson for awakening our interest in this problem and Dr. W. F. Huebner for discussion of his analytic approach. This work was supported in part by NSF Grant No. PHY-74-03531-A03.

---

*Present address: 14112 Castle Bd., Apt. 103, Silver Springs, Md. 20904.

[1]S. D. Oh, J. McEnnan, and R. H. Pratt, Phys. Rev. A 14, 1428 (1976).
[2]J. McEnnan, L. Kissel, and R. H. Pratt, Phys. Rev. A 13, 532 (1976); 2325(E) (1976).
[3]J. McEnnan, L. Kissel, and R. H. Pratt, Phys. Rev. A 14, 521 (1976).
[4]T. B. Lucatorto and T. J. McIlrath, Phys. Rev. Lett. 37, 428 (1976).
[5]T. J. McIlrath and T. B. Lucatorto, Phys. Rev. Lett. 38, 1390 (1977).
[6]D. W. Missavage and S. T. Manson, Phys. Lett. 38A, 85 (1972).
[7]F. Combet Farnoux and M. Lamoureux, Phys. Lett. 43A, 183 (1973).
[8]R. L. John and D. J. Morgan, Phys. Lett. 45A, 135 (1973).
[9]G. R. Daum and H. P. Kelly, Phys. Rev. A 13, 715 (1976).
[10]F. Combet Farnoux and M. Lamoureux, J. Phys. B 9, 897 (1976).
[11]A. Msezane, R. F. Reilman, S. T. Manson, J. Swanson, and L. Armstrong, Jr., Phys. Rev. A 15, 668 (1977).
[12]K. D. Chao, J. L. Dehmer, U. Fano, M. Inokuti, S. T. Manson, A. Msezane, R. F. Reilman, and C. E. Theodosiou, *Beam-Foil Spectroscopy* (Plenum, New York, 1976), Vol. 2.
[13]D. W. Missavage, S. T. Manson, and G. R. Daum, Phys. Rev. A 15, 1001 (1977).
[14]W. F. Huebner, M. F. Argo, and L. D. Ohlsen, J. Quant. Spectrosc. Radiat. Transfer 19, 93 (1978).
[15]R. H. Pratt and H. K. Tseng, Phys. Rev. A 5, 1063 (1972).
[16]For $-T_s \leq \omega \leq -T_c$, ν is imaginary, replace $\pi\nu/(e^{2\pi\nu}-1)$ by 0 and $\tan^{-1}(n/\nu)$ by $\frac{1}{2}\ln[(\nu+n)/(\nu-n)]$.
[17]F. Herman and S. Skillman, *Atomic Structure Calculations* (Prentice-Hall, Englewood Cliffs, N.J., 1963).
[18]The fit is not strongly sensitive to variations in the position of the endpoint near zero. On the other hand, there is considerable variation in the V_k if changes are made in the position of the extreme endpoint.
[19]This scaling can be derived, for example, by assuming that the universal neutral charge distribution in the ionic case is attenuated by a universal function $g(\lambda r/\lambda R)$, with $R(Z_i/Z)$.
[20]R. H. Pratt, Phys. Rev. 119, 1619 (1960).
[21]Y. S. Kim, S. D. Oh, and R. H. Pratt, Phys. Rev. A 18, 194 (1978).